Journal of Computer-Aided Molecular Design (2005) 19: 385–400
DOI 10.1007/s10822-005-7927-4

Construction of 4D-QSAR models for use in the design of novel p38-MAPK inhibitors

Nelilma Correia Romeiro[a,b,*], Magaly Girão Albuquerque[a]
Ricardo Bicca de Alencastro[a], Malini Ravi[b] & Anton J. Hopfinger[b]
[a]*Departamento de Química Orgânica, Laboratório de Modelagem Molecular (LabMMol), Instituto de Química, Universidade Federal do Rio de Janeiro, Centro de Tecnologia, Bloco A, Ilha do Fundão, 21949-900Rio de Janeiro, RJ, Brasil;* [b]*Department of Medicinal Chemistry and Pharmacognosy, Laboratory of Molecular Modeling and Design (LMMD), M/C 781, College of Pharmacy, The University of Illinois at Chicago, 833 South Wood Street, Illinois, Chicago, 60612-7231, USA*

Received 16 February 2005; accepted 22 May 2005

Key words: 4D-QSAR, anti-inflammatory drugs, inflammation, p38-MAPK, pyridinyl-imidazole, SB−203580

Summary

The p38-mitogen-activated protein kinase (p38-MAPK) plays a key role in lipopolysaccharide-induced tumor necrosis factor-α (TNF-α) and interleukin−1 (IL−1) release during the inflammatory process, emerging as an attractive target for new anti-inflammatory agents. Four-dimensional quantitative structure-activity relationship (4D-QSAR) analysis [Hopfinger et al., J. Am. Chem. Soc., 119 (1997) 10509] was applied to a series of 33 (a training set of 28 and a test set of 5) pyridinyl-imidazole and pyrimidinyl-imidazole inhibitors of p38-MAPK, with IC_{50} ranging from 0.11 to 2100 nM [Liverton et al., J. Med. Chem., 42 (1999) 2180]. Five thousand conformations of each analogue were sampled from a molecular dynamics simulation (MDS) during 50 ps at a constant temperature of 303 K. Each conformation was placed in a 2 Å grid cell lattice for each of three trial alignments. 4D-QSAR models were constructed by genetic algorithm (GA) optimization and partial least squares (PLS) fitting, and evaluated by leave-one-out cross-validation technique. In the best models, with three to six terms, the adjusted cross-validated squared correlation coefficients, Q^2_{adj}, ranged from 0.67 to 0.85. Model D ($Q^2_{adj} = 0.84$) was identified as the most robust model from alignment 1, and it is representative of the other best models. This model encompasses new molecular regions as containing pharmacophore sites, such as the amino-benzyl moiety of pyrimidine analogs and the N1-substituent in the imidazole ring. These regions of the ligands should be further explored to identify better anti-inflammatory inhibitors of p38-MAPK.

Introduction

Lipopolysaccharide (LPS), a component of the cell wall of gram-negative bacteria, induces macrophages to produce the pro-inflammatory cytokine tumor necrosis factor-α (TNF-α) and interleukin-1 (IL-1), key factors in immune responses against infection [1]. However, the uncontrolled production of these pro-inflammatory cytokines may generate chronic inflammatory diseases such as rheumatoid arthritis [2]. Amongst the most attractive targets in drug discovery for the suppression of LPS-induced synthesis of TNF-α and release of IL−1, p38-mitogen-activated protein kinase (p38-MAPK) [3–7] has been the focal point of many studies involving the search for new anti-inflammatory agents [8–16].

*To whom correspondence should be addressed. Fax: +21-2560-2518, E-mail: nelilma@far.fiocruz.br

The co-crystal structure of p38-MAPK with SB-203580 (4-(4-fluorophenyl)-2-(4-methylsulfinylphenyl)-5-(4-pyridyl)-1*H*-imidazole) (**1a**, Figure 1), the prototype inhibitor of the pyridinyl-imidazole class and other analogous compounds, showed that these inhibitors partially occupy the ATP binding site, preventing further phosphorilation of p38-MAPK [17, 18].

The most important interactions observed between p38-MAPK and SB-203580 in the co-crystal structure are (Figure 1): (i) a hydrogen bond between the N3 of the imidazole core and a hydrogen atom of the –NH2 group of Lys53 (N–N distance = 2.92 Å); (ii) a hydrogen bond between the N4 of the pyridine ring and the hydrogen atom of the N–H group of the peptide backbone of Met109 (N–N distance = 2.75 Å), something, which is also observed for the ATP adenosine ring; and (iii) a π-stacking interaction between the phenyl ring of the methylsulfinylphenyl moiety and the phenyl ring of Tyr35. Additionally, the 4-fluorophenyl ring of SB-203580 binds in a cavity close to Thr106, which is mostly composed of hydrophobic residues, and located behind and orthogonally to the ATP binding site [17, 18].

Liverton and co-workers have recently reported the synthesis and the anti-inflammatory activity evaluation of a series of potent and selective substituted imidazole inhibitors of p38-MAPK [16], which are improved analogues of compound **1a** (IC_{50} = 39 nM) (SB-203580, Figures 2 and 3), the prototype p38-MAPK inhibitor. One of the most potent inhibitors in this series, compound **4g** (IC_{50} = 0.19 nM) (Figure 3), shows good oral bioavailability in rat and rhesus monkeys, and reduces disease significantly in a rat adjuvant-induced arthritis model [16].

Three-dimensional (3D) quantitative structure–activity relationship (QSAR) studies can be useful in the search for sites on molecules that can be modified to make the molecules better specific ligands [19–22]. Among the 3D-QSAR methods, the receptor-independent (RI) 4D-QSAR method, proposed by Hopfinger and co-workers [23–29], is advantageous because it can incorporate molecular flexibility and multiple alignments, allowing the identification of the conformation that maximizes the predicted activity using the best 4D-QSAR model [26]. This conformation is defined as the active (or bioactive) conformation [26].

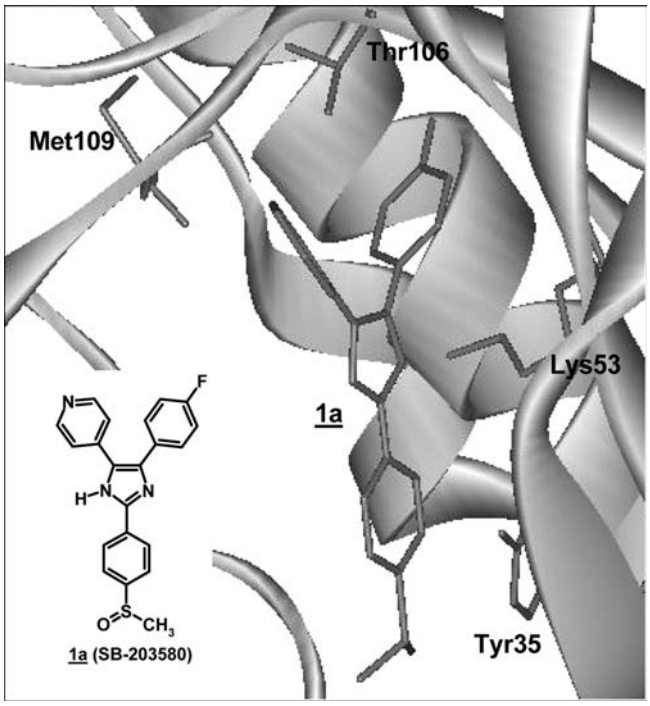

Figure 1. A close-up view of the active site of the crystallographic structure of **1a** (SB−203580) bound to p38-MAPK [18]. Only the main interacting residues are shown.

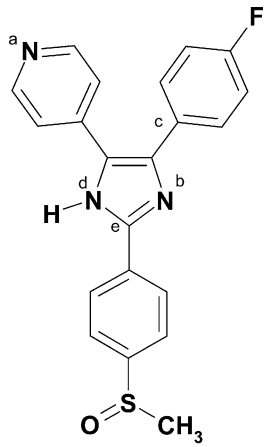

1a (7.41)

Alignment	1st atom	2nd atom	3rd atom
1	a	b	c
2	a	d	e
3	d	a	c

Figure 2. Three-ordered atom letter codes used in the 4D-QSAR analysis defining the three test alignments. Compound **1a** (pIC_{50} = 7.41) [16, 17], the prototype p38-MAPK inhibitor (SB–203580), is used to define the atom letter code.

The detailed formalism of the 4D-QSAR method has been published elsewhere [26]. Therefore, the main purpose of this study is to use the 4D-QSAR method to map the interaction sites of the series of inhibitors developed by Liverton and co-workers [16], and to propose structural changes in these p38-MAPK inhibitors to make them more potent and, thereby, better anti-inflammatory agents.

Methods

Biological data

The relative potency of 33 imidazole p38-MAPK inhibitors (**1a**, **2a**–**t**, **3a**–**d**, **4a**–**g**, and **5a**) (Figures 2 and 3) was reported as IC_{50}, measured on the purified enzyme [16]. The IC_{50} values ranges from 0.11 to 2100 nM, with the amino-benzyl substituted pyrimidine compounds demonstrating higher potency against this enzyme than the corresponding pyridine compounds [16]. The IC_{50} (nM) values were converted to molar units, and then expressed in negative logarithmic units, pIC_{50} (Figures 2 and 3). The pIC_{50} values ranges from 5.68 to 9.96 logarithm unities, and the plot of the pIC_{50} values revealed a homogeneous distribution of the activity values throughout the whole potency range of this series (data not shown), making it adequate for QSAR studies. The 4D-QSAR models were developed using a set of 28 compounds (training data set), randomly selected from the original 33 compounds. The best models were externally validated with the use of five compounds (***2e***, ***2i***, ***2l***, ***3a***, and ***4a***) (evaluation or test data set), randomly selected from the original 33 compounds, which were not included in the 4D-QSAR models development process. Care was taken to include all classes of compounds in both the training and test data sets.

4D-QSAR analysis

Structures building and conformational sampling by molecular dynamics

The three-dimensional (3D) structures of each of the 32 compounds (Figure 3) were based on the structure of compound **1a** (SB-203580, Figures 1 and 2), co-crystallized with p38-MAPK [18], taken from the Protein Data Bank (PDB) [30], under PDB code 1A9U. This structure is the bound conformation to the enzyme active site, or the *active conformation* of compound **1a**. A 3D model

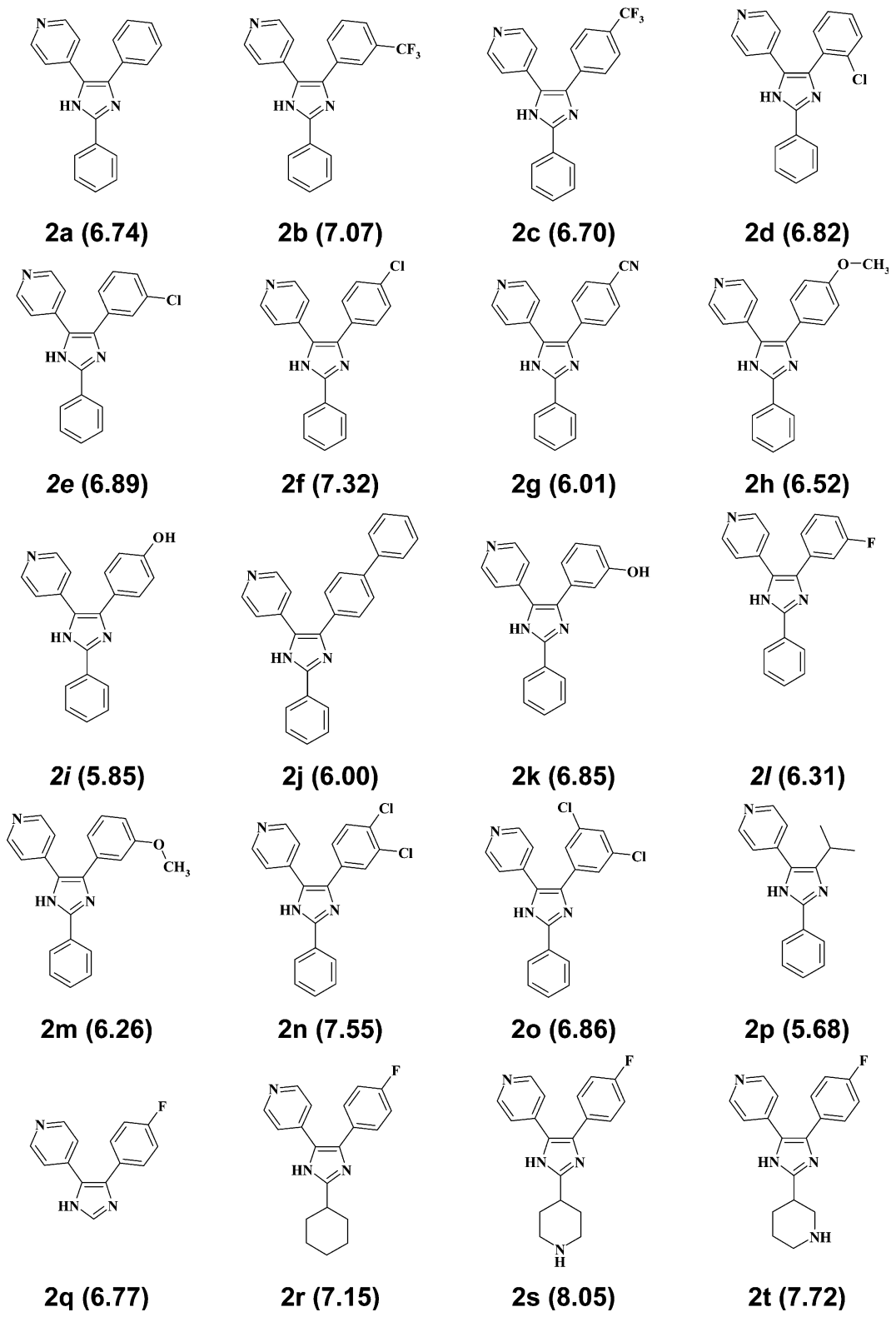

Figure 3. Compounds **2a**–**2t**, **3a**–**3d**, **4a**–**4g**, and **5a** (pIC_{50}) developed by Liverton et al. (1999) [16]. Training set compounds are in bold, and test set compounds in bold italics.

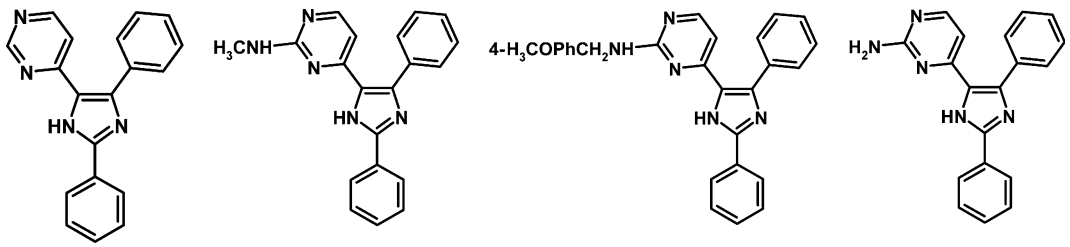

***3a* (6.15)** **3b (6.92)** **3c (7.42)** **3d (7.24)**

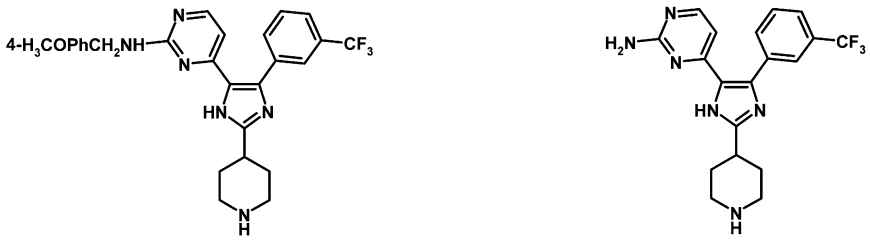

***4a* (8.12)** **4b (8.15)**

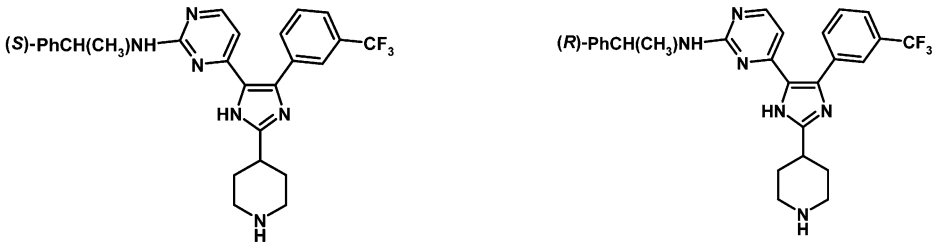

4c (9.12) **4d (9.01)**

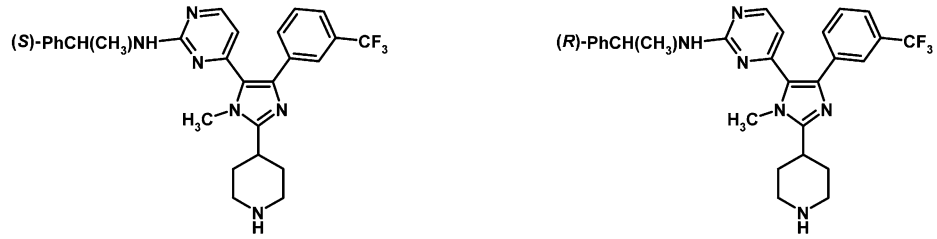

4e (9.96) **4f (8.82)**

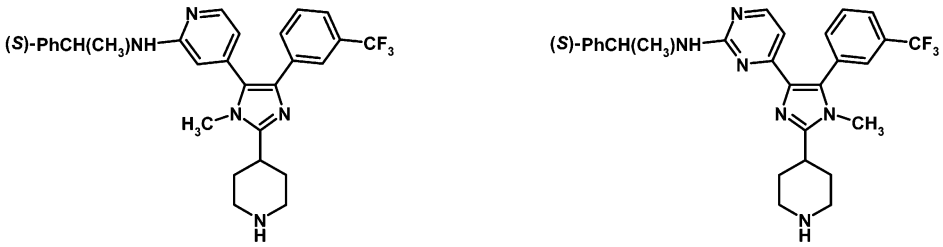

4g (9.72) **5a (5.91)**

Figure 3. Continued.

for each compound was constructed using the Builder module available in the Insight II molecular modeling package [31], based on the bound conformation of compound **1a** in complex with the enzyme. Each molecule was modeled in its neutral form, even compounds **2s**, **2t**, **4a**–**4g**, and **5a** (Figure 3) that have the piperidine group (the piperidinium cation has a pKa $\sim$11), because we are modeling the unbound ligands, i.e., the protein amino acid residues are not being considered in the calculations. Therefore, in the molecular dynamics simulation (MDS) step, the protonated forms would not have their counterparts and we would have conformational artifacts.

The 3D model for each structure was subsequently energy-minimized and the partial atomic charges were obtained using the AM1 [32] semi-empirical method available in the Insight II package [31]. The AM1 optimized structures were used as the initial structures in each molecular dynamics simulation (MDS) used to construct the conformational ensemble profile (CEP) of each ligand. The MDS was performed using the 4D-QSAR program [33] and the Molsim 3.0 software [34] with an extended MM2 force field [35], considering each structure in the vacuum and applying a distance-dependent dielectric function ($\varepsilon_r = D^*r_{ij}$) of 3.5^*r_{ij}. The temperature for the MDS was set at 303 K, the temperature at which the biological essays were performed [16]. Fifty thousand MDS steps were applied to each compound, with a step size of 0.001 ps, totaling a sampling time of 50 ps and 50,000 conformations for each molecule. An output trajectory file (the molecular internal coordinates of each conformation and the potential energy associated) was recorded every 10 steps (0.01 ps) with a total of 5000 frames, or sampling steps (conformations), composing the CEP of each ligand.

Grid cell size and alignment definitions

The CEP for each compound was overlaid onto a cubic lattice of a selected grid cell size, according to each selected alignment. The cubic lattice serves to record the distribution of spatial occupancy of each atom of each ligand in the training and/or test set. The grid cell size was defined as 2 Å, which corresponds to the integral number closest to twice the hydrogen atom van der Waals radii (r_{vdW} = 1.2 Å) and thus, is large enough to encompass a hydrogen atom.

Three different three-ordered atom trial alignments were selected to define the lattice overlays, and five atoms were selected from the pharmacophoric groups of the ligands identified by structure-activity relationship (SAR) [16] and crystallographic studies [17, 18] in order to define the alignments. The three-ordered atom alignment definitions are given in Figure 2, using compound **1a** as a reference.

Using the co-crystal structure of p38-MAPK with 1a (SB-203580) [18], alignment 1 is the atom sequence "**a**–**b**–**c**" (Figure 1), where atom "**a**" corresponds to N4 from the 5-pyridyl-, or 5-pyrimidyl-imidazole, which interacts, by hydrogen bonding, with the hydrogen atom of N-H group of the peptide backbone of Met109. Atom "**b**" is the N3 of the imidazole core which interacts by hydrogen bonding with the hydrogen atom of the –NH2 group of Lys53. Atom "**c**", though not interacting specifically with any of the atoms, orientates the 4-Aryl group to a hydrophobic pocket close to Thr106.

Alignment 2 is the atom sequence "**a**–**d**–**e**", where atom "**d**" corresponds to N1 from the imidazole ring, which has no specific interaction with the crystal structure, but lies close to the carbonyl group of the peptide backbone of Met109, and could interact with it during the MDS by hydrogen bonding. Atom "**e**", though not interacting specifically with any of the atoms, orientates the 2-Aryl group to an aromatic residue. As occurs in the crystal structure of **1a**, there is π-stacking between the phenyl ring of the methylsulfinylphenyl moiety of **1a** and the phenyl ring of Tyr35. Finally, alignment 3 is the atom sequence "**d**–**a**–**c**" that 'combines' alignments 1 and 2.

Interaction pharmacophore elements (IPEs) definition

The 4D-QSAR method [26, 33] currently defines seven types of interaction pharmacophore elements (IPEs), corresponding to atom types that may occupy the grid cells. These IPEs correspond to the interactions that may occur in the active site, and are related to the pharmacophore groups. In this study the seven types of IPEs available in 4D-QSAR program [33] were used and can be described as follows: (i) any type (any); (ii) nonpolar (np); (iii) polar-positive charge

(p+); (iv) polar-negative charge (p−); (v) hydrogen bond acceptor (hba); (vi) hydrogen bond donor (hbd); and (vii) aromatic systems (ar).

Grid cell occupancy descriptors (GCODs) generation

After each conformation from the CEP of each compound has been placed in the reference grid cell space according to the trial alignment (see Grid Cell Size and Alignment Definitions), the grid cell occupancy profiles for each of the chosen IPEs (see Interaction Pharmacophore Elements Definition) are then computed and used as the 4D-QSAR descriptors, which are named grid cell occupancy descriptors (GCODs). We have computed the absolute occupancy of each grid cell (*i*, *j*, *k*), where *i*, *j*, and *k* define the *xyz*-coordinate location in Cartesian space of the grid cell, at time t in the MDS ensemble sampling for the IPE atoms of each compound [26]. The absolute occupancy is the number of times (in the time-length of the MDS ensemble sampling) that each IPE atoms of a molecule are "in" the cell. The "in" a grid cell corresponds to the geometric center of the test atom residing anywhere within the grid cell [26].

The absolute occupancy measures were normalized by dividing the sampling values by the number of sampling steps (conformations from the MDS, see Structures Building and Conformational Sampling by Molecular Dynamics). The 4D-QSAR scheme intrinsically defines the complete set of grid cells to include in an analysis [26]. The composite set of grid cells occupied at least once in constructing the CEP for the all atom IPE of each member of the training set defines the complete set of grid cells [26]. This set of GCODs constitutes the complete set of independent variables used in the construction of the 4D-QSAR models, and it was assigned as the "original databank".

Data reduction

4D-QSAR analysis generates an enormous number of QSAR descriptors because of the large number of grid cells and because of the IPEs [26], therefore, in order to exclude data noise or useless data from the GCODs data set (original databank or databank 1, DB1), we have considered two subsequent levels of data reduction available in the 4D-QSAR program [23, 26, 33].

The first eliminates GCODs whose variance (self-variance) over the set of analogues was less then a pre-chosen cutoff value. In this case, five databanks, DB2-DB6, were built from DB1, eliminating GCODs that showed variance cutoff values of up to 0.1, 0.3, 0.5, 1.0, and 1.5, respectively. These trial cutoff values were chosen according to the variance observed in the training data set, that ranged up to 1.7 and represents a filter to eliminate nonsignificant occupancies of the cells, which would possibly mean noise in the further regression analysis.

The second level of data reduction employed partial least squares (PLS) regression models optimized as a function of the number of principal components to identify the most highly weighted GCODs from the population of available GCODs from the first filtering procedure described above. Therefore, the DB1 and the five DBs derived from DB1 were then separately submitted to PLS analysis as implemented in the 4D-QSAR program [33]. This procedure was used to prune each DB by identifying and selecting only the most highly weighted PLS GCODs (descriptors) that would be used in the subsequent 4D-QSAR step (GA analysis).

4D-QSAR model calculation: GA-PLS approach

The GCODs with the highest weight on each DB from the PLS data reduction, were optimized using the GA-PLS approach [36, 37], implemented in the 4D-QSAR program [33]. The genetic function approximation (GFA) algorithm [36], in the GA-PLS approach, combines Holland's genetic algorithm (GA) and Friedman's multivariate adaptive regression splines (MARS) algorithm [38], and it is implemented with partial least-squares (PLS) regression analysis [37].

Concisely, in the GA-PLS approach [36, 37], initial models (equations) are generated by randomly selecting some features (descriptors) from the training data set, building basis functions (terms) from these descriptors using user-defined basis function types (e.g. linear), and then constructing a population of QSAR-genetic models (equations) from random sequences of these basis functions. Improved models are constructed by performing crossover operation to recombine the terms of the better-scored models, according the Friedman's lack-of-fit (LOF) measure (Equation (1)) [36–38]:

$$\mathrm{LOF} = \frac{\mathrm{LSE}}{(1 - \frac{c+dp}{M})^2} \quad (1)$$

In Equation (1), LSE is the least-squares error; c is the number of basis functions (terms) in the model (equation); d is the smoothing factor (larger values of d leads to models with fewer terms); p is the number of features contained in all basis functions (in this work, each base function corresponds to just one descriptor or independent variable); and M is the number of compounds in the training set [36, 37]. The LOF score is a penalized LSE measure, i.e., when two models have the same value of LSE, that one which has the lowest number of terms will have the lowest (best score) value of LOF [36, 37].

In addition to crossover operations, a rate of mutation operation is allowed, in order to ensure some degree of diversity to the population. At the end of optimization process (evolution), the LOF value remains essentially invariable over crossover operations, and the QSAR models have stabilized [36,37].

The optimizations of the GCODs with the highest weight on each DB from the PLS data reduction were initiated using 100 randomly generated models (equations), each model having initially four variables (terms), and each term corresponding to just one descriptor (independent variable). Mutation probability over the crossover optimization was set at a rate of 10%, and the smoothing factor (variable d in Equation (1)), which controls the number of independent variables in the models, was arbitrarily adjusted in order to find equations with at least three terms but no more than six terms. Three components were used for the PLS regression, and 10,000 to 20,000 crossover operations were allowed in the model optimizations.

Internal and external 4D-QSAR model validation

The ten best scored models found by GA-PLS analysis [36, 37], according to their values of Friedman's LOF measure [38], were then submitted to internal validation by the leave-one-out (LOO) cross-validation method available in the 4D-QSAR program [33]. The main statistical parameters evaluated were [36–40]: R^2 (squared correlation coefficient), SE (standard error), Q^2 (leave-one-out cross-validated R^2), F (Fischer's test of statistical significance), LOF (Friedman's lack-of-fit score), residuals (observed minus calculated pIC_{50} values), and s (standard deviation of the residuals). Compounds where residuals were greater than twice the standard deviation of the residuals have been considered as outliers. Each alignment was evaluated using the procedure described above.

The best models were externally validated with the use of five compounds (***2e***, ***2i***, ***2l***, ***3a***, and ***4a***) (evaluation or test data set), which were not included in the 4D-QSAR model development. These compounds were used to test the 4D-QSAR best models for their ability to predict biological activities values of compounds not included in the training data set.

4D-QSAR model and bioactive conformation selections

A final optimized 4D-QSAR model was selected taking into consideration alignment and statistical fitting parameters. The lowest-energy conformer state (up to 2.0 Kcal/mol from the minimum energy conformation), from the set sampled for each compound, which predicted the maximum potency using the optimum 4D-QSAR model, was defined as the active conformation [26]. The putative bioactive conformations obtained were manually docked to the active site of p38-MAPK (PDB code 1A9U) using the Insight II molecular modeling package [31], in order to check for possible interactions with the surrounding amino acid residues.

Results

Alignments comparison

In order to identify the best alignment, a plot of the best adjusted cross-validated R^2 (Q^2_{adj}) [38] obtained in the 4D-QSAR analysis was made for the three alignments considered in this study, irrespective of which DB was used (Figure 4). The plot in Figure 4 shows that alignments 1 and 2 generated the best models and alignment 3 had the poorest performance, irrespective of the number of terms (three to six independent variables) in each equation (model). This finding is consistent with alignments 1 (atoms "**a**–**b**–**c**") and 2 (atoms "**a**–**d**–**e**") having the same initial atom "**a**" (Figure 2)

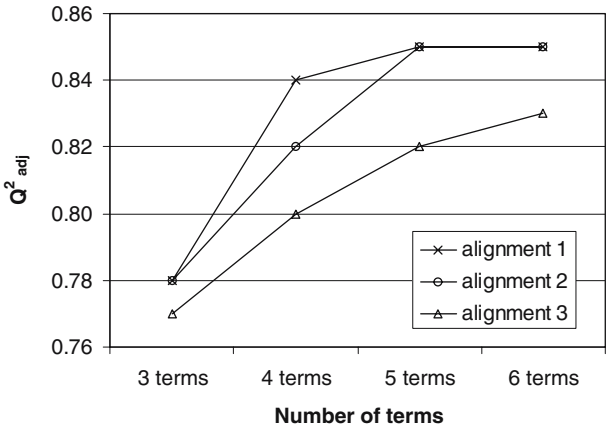

Figure 4. Plot of Q^2_{adj} from the best model versus number of descriptors (terms) in the model for alignments 1, 2 and 3.

that corresponds to N4, which interacts with the peptide backbone of Met109 (Figure 1). Thus, only the results obtained from alignments 1 and 2 are discussed from this point forward.

The analysis of the Q^2_{adj} plot for alignments 1 and 2 (Figure 4) shows that the best Q^2_{adj} values were those of the six term models. However, both the three and six term models in this analysis were not considered because the three-term model is poor and, since the training set is composed of only 28 compounds, the six term models may be over fitting the data. The criteria used to select the best models of each alignment were as follows: (i) models with four or five terms; (ii) models with values of $Q^2_{adj} \geq 0.80$; and (iii) models with the highest Q^2_{adj} values.

Alignment 1 analysis

Following the criteria described above, models A–D of alignment 1 were selected from DBs 1, 2, 5 and 6, respectively (Table 1) for detailed analysis. A general view of these models makes clear that the majority of grid cells are occupied by IPEs related to any type (eight GCODs of type any) and nonpolar atoms (five GCODs of type np), representing unspecific and nonpolar interactions, respectively, even though there are a few grid cells

Table 1. The best 4D-QSAR models obtained from alignment 1, using DB1 (A, 4 terms), DB2 (B, 5 terms), DB5 (C, 5 terms) and DB6 (4 terms) for the training set of 28 inhibitors of p38-MAPK [16].

Model	Equation
A	pIC_{50} = 7.07 + 8.51(−1,−3,4)(p+) + 5.08(−1,−1,−2)(any) + 1.38(−1,−1,5)(any) − 1.07(0,0,4)(np) N = 28, R^2 = 0.87 SE = 0.15 Q^2 = 0.85 F = 0.65 LOF = 0.37
B	pIC_{50} = 6.78 + 28.00(−1,1,−1)(any) + 17.34(1,−2,5)(p+) − 3.53(1,1,4)(np) − 2.14(−1,0,−1)(np) + 1.12(−1,−1,0)(any) N = 28, R^2 = 0.89, SE = 0.14, Q^2 = 0.85, F = 0.43, LOF = 0.25
C	pIC_{50} = 8.41 + 1.50(1,−2,4)(any) + 1.49(−1,−1,0)(any) − 1.38(0,0,4)(any) − 0.47(0,−1,0)(np) − 1.01(0,−1,3)(any) N = 28, R^2 = 0.88, SE = 0.15, Q^2 = 0.84, F = 0.46, LOF = 0.30
D	pIC_{50} = 6.67 + 3.30(1,0,−1)(np) + 8.29(−1,−2,2)(any) − 1.26(0,0,4)(np) + 1.48(−1,−2,4)(any) N = 28, R^2 = 0.88, SE = 0.14, Q^2 = 0.86, F = 0.61 LOF = 0.24

N = number of compounds in the training data set; R^2 = squared correlation coefficient; SE = standard error; Q^2 = leave-one-out cross-validated R^2; F = Fischer's test of statistical significance; LOF = Friedman's lack-of-fit score.

occupied by atoms of the polar-positive charge type (two GCODs of type p+), representing polar interactions. These data suggest a predominance of nonpolar ligand–receptor interactions in this series of inhibitors as the most important feature to be observed in the design of new p38-MAPK analog inhibitors.

In order to determine if the information in the models for each alignment is redundant, the cross-correlation matrix of the residuals of fit of the selected models of alignment 1 (Table 2) was computed. The results show that the models are highly correlated as was observed for models A and D (R = 0.80) and C and D (R = 0.77). These correlations are probably due to spatially identical grid cells, such as GCOD (0,0,4), which is present in models A, C, and D (Table 1). Model D, which has the highest cross-correlation, seems to incorporate information from the other three models.

In order to gain a better understanding of the behavior of the fitted data to the models, the descriptors of models A–D (Table 1) were inspected in detail. For example, GCOD (0,0,4), which is present in models A, C, and D, is occupied by nonpolar atoms (np) in models A and D, and by any atom type (any) in model C, always with a negative regression coefficient, suggesting that occupation of this region is detrimental to the potency. Also, GCOD (−1,−1,0) is present in models B and C as any type of atom, with positive regression coefficients in both models, showing an activity-enhancing profile. Finally, GCODs (1,−2,4) and (−1,−2,4), which are close in space, are present in models C and D, respectively, as any type of atom, with positive regression coefficients. These observations reinforce the fact that the models are highly correlated, according to the results of the cross-correlation matrix of the residuals of fit (Table 2).

Table 2. Cross-correlation coefficients of the residuals of fit for models A–D obtained in the 4D-QSAR analysis using alignment 1.

Models	A	B	C	D
A	**1.00**			
B	0.72	**1.00**		
C	0.74	0.62	**1.00**	
D	0.80	0.73	0.77	**1.00**

In addition, the cross-correlations between the descriptors in each model were computed and no GCOD was found to correlate significantly to any other (data not labeled). However, a closer inspection of the descriptors and analysis of intercorrelation in the models showed that GCOD (0,0,4)(np) is identical in models A and D, and GCOD (−1,−1,0)(any) is present in models B and C. Moreover, there is a significant spatial correlation between GCODs (0,0,4)(any) and (−1,−2,4)(any), of models C and D, with R-value equals to 0.53. These results confirm that model D incorporates the information within the other models, and that model B is the least correlated and general feature model.

GCOD (−1,−3,4)(p+) of model A (Table 1) is occupied by only one compound. This grid cell is taken as a ''spurious'' variable, which is included in the regression equation to improve the fit for this single training set compound. Thus, model A has been eliminated from the final selection of the most representative model(s) of alignment 1.

Finally, internal and external validation of models B–D, which consists of the calculations of the standard deviations of the residuals of fit for the training set, and then both the training and the evaluation sets (Table 3), were performed. The analysis of the standard deviations of the training and evaluation sets shows that models B and D are best using alignment 1. The analysis of the data showed that model B has three outliers (**2b**, **2j** and **2n**), models C (**2f** and **2r**) and D (**2f** and **2n**) two outliers for the training set (28 compounds). When the whole set of compounds (33 compounds) are used to build corresponding models, model B has only one outlier, ***2i***, from the evaluation set; model C has two outliers (**2f** and **2r**), both from the training set; and model D has no outliers. Based upon these results, models B and D were selected

Table 3. Standard deviation values of the residuals of fit obtained for models B–D in the 4D-QSAR analysis using alignment 1.

Model[a]	s	Outliers	s'	Outliers'[b]
B	0.35	**2b**, **2j**, **2n**	0.38	***2i***
C	0.39	**2f**, **2r**	0.39	**2f**, **2r**
D	0.35	**2f**, **2n**	0.38	–

[a]s and outliers considering only the training set (28 compounds); s' and outliers' including the evaluation set (33 compounds);
[b]Compounds of the evaluation set in italics.

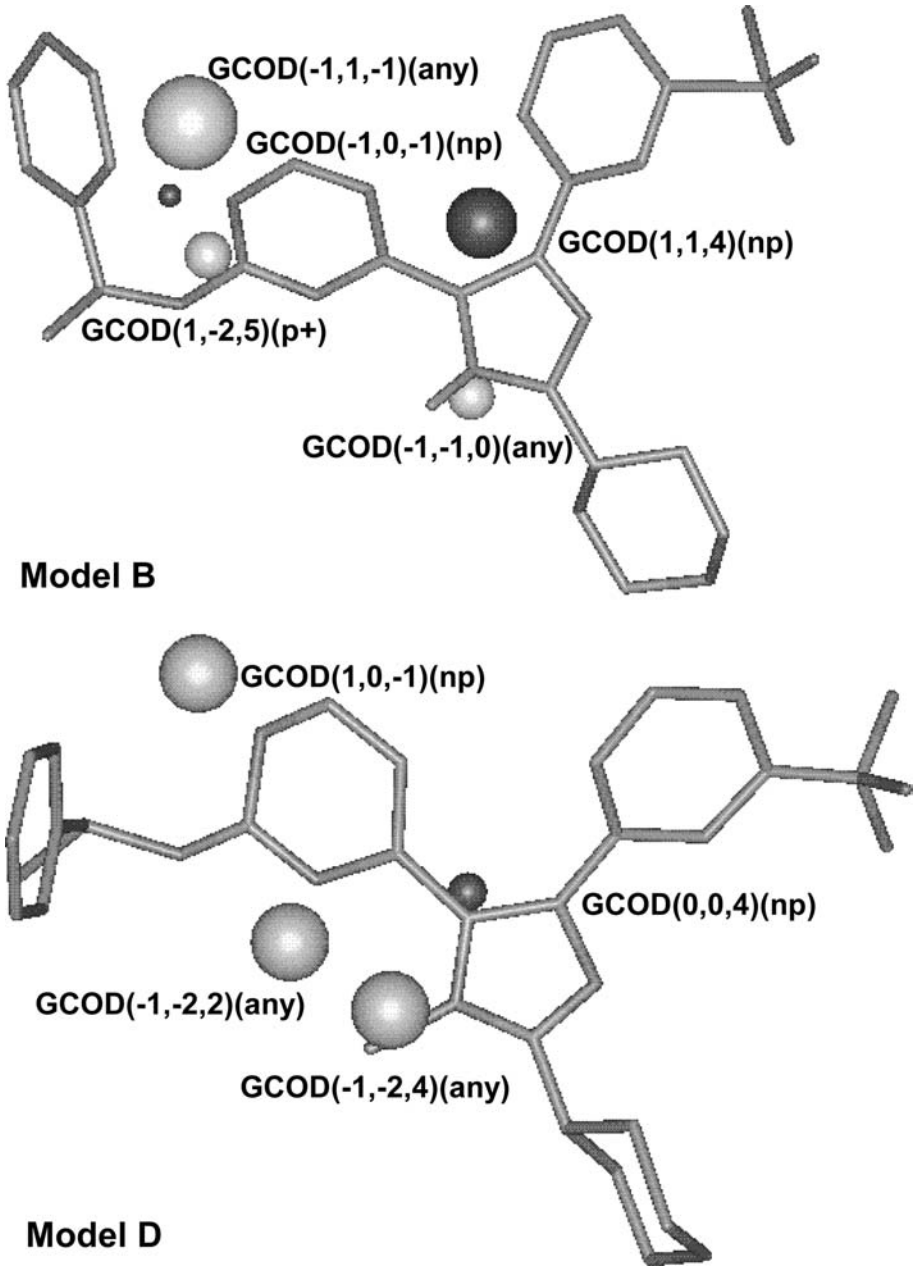

Figure 5. Models B and D obtained by 4D-QSAR from alignment 1 using compound **4e** as a reference. Light spheres indicate activity-enhancing pharmacophore sites and dark spheres indicate activity-decreasing pharmacophore sites.

as the most representative models of alignment 1. Compound **4e** (the most potent compound in the series) with its postulated active conformation was used as the reference structure in order to display models B and D (Figure 5) with their GCODs represented as light (positive coefficient) and dark (negative coefficient) spheres. Figure 6 shows the plot of observed versus predicted pIC_{50} values obtained with the best models from alignment 1: Model B and Model D.

Alignment 2 analysis

The same criteria used to select and evaluate the models generated with alignment 1 were used to evaluate alignment 2. The best models with respect

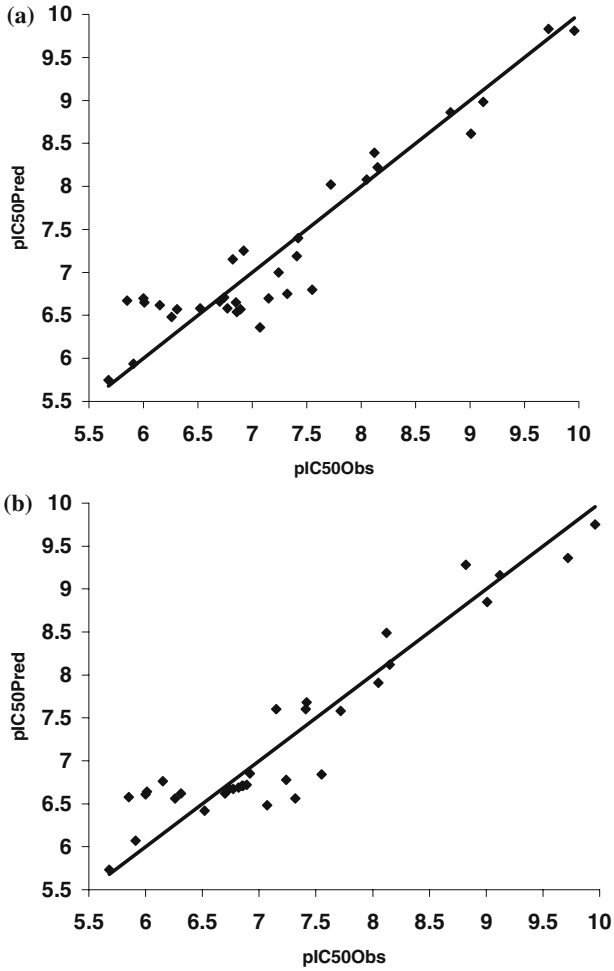

Figure 6. Plot of observed versus predicted pIC_{50} values obtained with the best models from aligment 1: (a) Model B and (b) Model D.

Table 4. The best 4D-QSAR models obtained from alignment 2, using DB1 (E, 5 terms), DB3 (F, 4 terms) and DB4 (G, 5 terms) for the training set of 28 inhibitors of p38-MAPK [16].

Model	Equation
E	pIC_{50} = 6.10 + 20.61(−1,−1,5)(p+) + 3.54(−1,−1,0)(hbd) − 1.46(−1,4,3)(np) + 4.98(1,−1,2)(np) + 4.58(2,0,5)(any) N = 28, R^2 = 0.90, SE = 0.12, Q^2 = 0.85, LOF = 0.25
F	pIC_{50} = 6.33 + 5.19(2,−1,5)(any) + 6.86(0,−1,5)(hba) + 3.48(1,−1,2)(any) + 1.64(−1,0,5)(any) N = 28, R^2 = 0.86, SE = 0.16, Q^2 = 0.84, LOF = 0.28
G	pIC_{50} = 5.31 + 3.43(−1,0,−2)(any) − 8.62(−1,2,4)(np) − 1.85(−2,3,2)(any) − 4.91(0,−1,5)(np) + 3.12(0,0,4)(any) N = 28, R^2 = 0.90, SE = 0.11, Q^2 = 0.87, LOF = 0.19

N = number of compounds in the training data set; R^2 = squared correlation coefficient; SE = standard error; Q^2 = leave-one-out cross-validated R^2; F = Fischer's test of statistical significance; LOF = Friedman's lack-of-fit score.

Table 5. Cross-correlation coefficients of the residuals of fit for models E–G obtained in the 4D-QSAR analysis of alignment 2.

Models	E	F	G
E	**1.00**		
F	0.81	**1.00**	
G	0.65	0.80	**1.00**

to these criteria are shown in Table 4. As in alignment 1, a general view of the models from alignment 2 demonstrates that the majority of grid cells represent unspecific and nonpolar interactions, since they are occupied by IPEs related to any type (seven GCODs of type any) and nonpolar atoms (four GCODs of type np). A few grid cells represent polar and hydrogen bond interactions, since they are occupied by IPEs related to polar-positive (one GCOD of type p+), hydrogen bond acceptor (one GCOD of type hba), and donor atoms (one GCOD of type hbd). These data reinforce the postulated predominance of nonpolar interactions in this series of compounds as the most important feature to be observed in the design of new p38-MAPK inhibitors.

The analysis of the cross-correlation matrix (Table 5) of the residuals of fit of the selected models show that all of the best models are highly correlated to one another, as observed for alignment 1 (Table 2). High correlation values for models E and F ($R = 0.81$), and F and G ($R = 0.80$), are probably due to spatially identical cells. For example, GCOD (1,−1,2), has an IPE corresponding to a nonpolar atom type (np) in model E and an any atom type in model F (Table 4), and positive regression coefficients in both models indicating its activity-enhancing profile. In addition, the analysis of the linear cross-correlation matrix (R) shows that the descriptors in each model are nearly orthogonal to one another (data not labeled). Based on these results, as observed in alignment 1 for model D, model F seems to "incorporate" the features of models E and G.

Table 6. Standard deviations of the residuals (s) of fit obtained for models E–G in the 4D-QSAR models from alignment 2.

Model[a]	s	Outliers	S′	Outliers′[b]
E	0.33	**2f**, **2q**	0.36	***2i***
F	0.39	**2p**	0.41	**2p**
G	0.30	**2f**	0.34	**2f**, ***3a***

[a]s and outliers considering only the training set (28 compounds); s' and outliers′ including the evaluation set (33 compounds);
[b]Compounds of the evaluation set in italics.

The cross-correlation coefficients among the descriptors in the different models (data not labeled) were computed. Except for grid cell (1,−1,2), which is identical in models E and F, and differs only in atom type (np and any in models E and F, respectively), the most correlated grid cells are the GCODs (−1,4,3)(np) of model E and (0,−1,5)(hba) of model F ($R = 0.53$). However, this particular cross-correlation seems to be a chance correlation, since grid cells are neither close nor occupied by similar atom types. Nevertheless, there is a possibility of a coupled conformational correlation over space arising through a common torsion angle, such as rotation about the bond joining the imidazole ring and the pyridine or the pyrimidine ring (Figures 2 and 3).

Finally, the performances of the models for the training and evaluation sets were characterized in terms of the residuals of the fit (Table 6), in the same manner as done for alignment 1 (Table 3). The standard deviations of prediction for the training set, and for all the compounds, suggests that models E and G are the best models for alignment 2 since they have the smallest standard deviations. There are two outliers for model E, compounds **2f** and **2q**, while models F and G both have only one outlier, compounds **2p** and **2f**, respectively. However, if all compounds (training and evaluation sets) are considered, models E and F have just one outlier, compounds ***2i*** (from the evaluation set) and **2p**, respectively, while model G has two outliers, compounds **2f** and ***3a***, the last one from the evaluation set. Therefore, model E is judged the best model for alignment 2, but is slightly less robust ($Q^2_{adj} = 0.82$) than models B ($Q^2_{adj} = 0.84$) and D ($Q^2_{adj} = 0.84$) from alignment 1. Consequently, alignment 1, overall, is superior to alignment 2.

Discussion

The models developed in this analysis suggest that alignment 1 yields the best results, both statistically

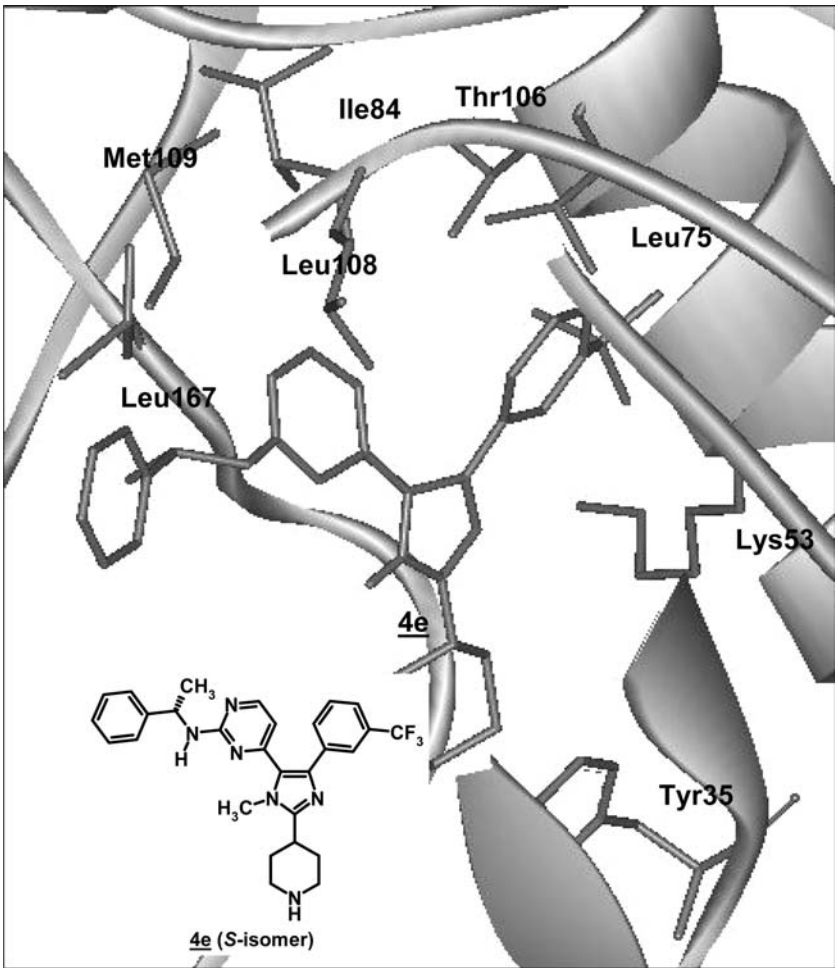

Figure 7. The postulated 4D-QSAR bioactive conformation from model D of compound **4e** docked in the active site of the crystal structure of p38-MAPK [18]. Only the main interacting residues are shown.

and qualitatively. Models B and D show a spatial correlation among their respective GCODs, although no significant correlation among these GCODs is observed in the GCOD cross-correlation matrix. Since model D has no outliers for the entire data set (Table 3), we have selected this model as the best one for the training set.

Besides, it showed lower values on its regression coefficients, which suggests a smooth distribution of the GCODs values appearing in the model in relation to the 28 compounds of the training set. This is in opposition to model B. For instance, model B has high values of coefficients for certain cells, indicating that a smaller number of compounds pertaining to the most potent range in the whole set is occupying that region in space; such as the cell (−1,1,−1)(any), occupied by only six compounds, and cell (1,−2,5)(p+), with occupancy values for some of the most potent compounds like 4f and 4g (data not labeled) equal or close to zero.

Additionally, the analysis of model D showed that the region in space occupied by the aminobenzyl substituent (–NHR) in position 2 of the pyrimidine ring, which is present in some compounds of series **3** and all the compounds of series **4**, both of them containing the most potent compounds of the training set, corresponds to an important pharmacophore site for the inhibitory activity of these compounds to p38-MAPK.

This region in space is represented by GCOD (1,0,−1)(np) of model D (Table 1, Figure 5), showing the highest frequency of occupation for the most potent compounds in the training set (**4c**–**4g**).

It corresponds to the methyl group of the lateral chain of the pyrimidine ring of those compounds. As an example, comparing **4a** (pIC_{50} = 8.12) with 4c (pIC_{50} = 9.12) or **4d** (pIC_{50} = 9.01) we could observe that the first compound, which does not has the methyl group, is less potent than the others (Figure 3). We could argue that the *p*-methoxy group in lateral chain of **4a** is the responsible for its lower potency, since **4c** and **4d** do not have substituents in the phenyl ring. However, among compounds of series **3**, compound **3d** is the only one that has the *p*-methoxy substituent, and it is the most potent in its own series.

Therefore, molecular modification in this region is a good target strategy to develop better anti-inflammatory agents, that is, more potent inhibitors of p38-MAPK. Examples of such modifications could be the replacement of the NH-alkyl-phenyl group by: NH-isopropyl, NH-cyclohexyl, NH-*tert*-butyl groups in order to verify the importance of the phenyl group; isobutyl group in order to verify the importance of the NH group; $NHCH_2$-piperidine, $NHCH_2$-piperazine groups in order to try to reach the Asp168 residue (7.6 Å distant from C2-pirimidine ring).

The region in space close to N-1 of the imidazole ring, represented in model D by GCOD (−1,−2,4) (any), can be occupied by nonspecific groups on the inhibitor (any IPE types) enhancing inhibition potency. It corresponds to hydrogen atom or methyl group attached to N1 of the imidazole ring. Such groups can come also from substituents in the region next to N-3 (or C-3 if the substituent is a pyridine ring) of the pyrimidine ring, represented by GCOD (−1,−2,2)(any). This SAR feature has also been pointed out from the SAR studies done by Liverton and colleagues [16].

Finally, the postulated active conformation of compound **4e**, the most potent member of the training set, as determined from the 4D-QSAR analysis, is assumed to be the bioactive conformation for the series of inhibitors represented by the training set. In addition, this postulated bioactive conformation was docked (Figure 7) into the region occupied by homologous pyrimidine compounds co-crystallized with human p38-MAPK [18]. As seen in Figure 7, a comparison of the amino acid residues which defines the binding pocket of these ligands to the GCODs obtained with model D (Figure 5) permits assignment of interactions between substituents of the ligands occupying cell (1,0,−1)(np) and nonpolar residues like the side chain of Met109 and Leu167 (Figure 7). However, future inhibitor design studies should focus on the length and volume of substituents in this nonpolar region in order to avoid repulsive steric interactions predicted by GCOD (−1,0,−1)(np) of model B (Figure 5). Also, repulsive steric interactions of ligand's substituents in the region corresponding to the location of the 3-trifluoromethyl-phenyl moiety of the bound active inhibitors with bulky residues in the region near Thr106, such as Leu108 (Figure 7), can be deleterious to inhibitory potency, as is predicted by GCOD (0,0,4)(np), found in model D (Figure 5).

The 4D-QSAR models developed in this study suggest novel molecular regions that can be explored in the search of better anti-inflammatory agents that act by inhibiting p38-MAPK. One such region is that occupied by the amino-benzyl moiety of pyrimidine analogs, and another is the region around N−1 in the imidazole ring. It is quite satisfying that the best 4D-QSAR model was obtained with alignment 1, using ligand regions that correspond to pharmacophoric groups already identified in the pyridinyl class of compounds. Thus, although there were only five compounds in the test set, and a larger test set would probably improve the predictive power of the selected model, it seems to be partly validated in addition to being robust and useful for the design of new p38-MAPK inhibitor.

Acknowledgements

NCR is grateful to Conselho Nacional de Desenvolvimento Científico e Tecnológico (CNPq, Brazil) for fellowship support. Resources of the Laboratory of Molecular Modeling and Design (LMMD) were used to perform these studies. Support from the Chem21 Group, Inc. is gratefully acknowledged. Special thanks to Manisha Iyer and Xuan Hong for the relevant comments on the 4D-QSAR methodology.

References

1. Newton, R.C. and Decicco, C.P., J. Med. Chem., 42 (1999) 2295.
2. Arend, W.P. and Dayer, J.M., Arthritis Rheum., 38 (1995) 151.

3. Raingeaud, J., Gupta, S., Rogers, J.S., Dickens, M., Han, J., Ulevitch, R.J. and Davis, R.J., J. Biol. Chem., 270 (1995) 7420.
4. Lee, J.C., Kumar, S., Griswold, D.E., Underwood, D.C., Votta, B.J. and Adams, J.L., Immunopharmacology, 47 (2000) 185.
5. Hale, K.K., Trollinger, D., Rihanek, M. and Manthey, C.L., J. Immunol., 162 (1999) 4246.
6. Han, J., Lee, J.D., Jiang, Y., Li, Z., Feng, L. and Ulevitch, R.J., Science, 265 (1994) 808.
7. Kyriakis, J.M. and Avruch, J., J. Biol. Chem., 271 (1996) 24313.
8. Cohen, P., Curr. Opin. Chem. Biol., 3 (1999) 459.
9. Gallagher, T.F., Seibel, G.L., Kassis, S., Laydon, J.T., Blumenthal, M.J., Lee, D., Boehm, J.C., Thompson-Fier, S.M., Abt, J.W., Sorenson, M.E., Smietana, J.M., Hall, R.F., Garigipati, R.S., Bender, P.E., Erhard, K.F., Krog, A.J., Hoffman, G.A., Sheldrake, P.L., McDonnell, P.C., Kumar, K.F., Young, P.R. and Adams, J.A., Bioorg. Med. Chem., 5 (1997) 49.
10. Boehm, J.C., Bower, M.J., Gallagher, T.F., Kassis, S., Johnson, S.R. and Adams, J.L., Bioorg. Med. Chem. Lett., 11 (2001) 1123.
11. de Laszlo, S.E., Visco, D., Agarwal, L., Chang, L., Chin, J., Croft, G., Forsyth, A., Fletcher, D., Frantz, B., Hacker, C., Hanlon, W., Harper, C., Kostura, M., Li, B., Luell, S., MacCoss, M., Mantlo, N., O'Neill, E.A., Orevillo, C., Pang, M., Parsons, J., Rolando, A., Sahly, Y., Sidler, K. and O'Keefe, S.J., Bioorg. Med. Chem. Lett., 8 (2000) 2689.
12. Mavel, S., Thery, I. and Gueiffier, A., Arch. Pharm. (Weinheim), 335 (2002) 7.
13. Redman, A.M., Johnson, J.S., Dally, R., Swartz, S., Wild, H., Paulsen, H., Caringal, Y., Gunn, D., Renick, J., Osterhout, M., Kingery-Wood, J., Smith, R.A., Lee, W., Dumas, J., Wilhelm, S.M., Housley, T.J., Bhargava, A., Ranges, G.E., Shrikhande, A., Young, D., Bombara, M. and Scott, W.J., Bioorg. Med. Chem. Lett., 11 (2001) 9.
14. Henry, J.R., Rupert, K.C., Dodd, J.H., Turchi, I.J., Wadsworth, S.A., Cavender, D.E., Schafer, P.H. and Siekierka, J.J., Bioorg. Med. Chem. Lett., 8 (1998) 3335.
15. Adams, J.L., Boehm, J.C., Kassis, S., Gorycki, P.D., Hall, R., Sorenson, M., Lee, J.C., Ayrton, A., Griswold, D.E. and Gallagher, T.F., Bioorg. Med. Chem. Lett., 8 (1998) 3111.
16. Liverton, N.J., Butcher, J.W., Claiborne, C.F., Claremon, D.A., Libby, B.E., Nguyen, K.T., Pitzenberger, S.M., Selnick, H.G., Smith, G.R., Tebben, A., Vacca, J.P., Varga, S.L., Agarwal, L., Dancheck, K., Forsyth, A.J., Fletcher, D.S., Frantz, B., Hanlon, W.A, Harper, C.F., Hofsess, S.J., Kostura, M., Lin, J., Luell, S., O'Neill, E.A, Orevillo, C.J., Pang, M., Parsons, J., Rolando, A., Sahly, Y., Visco, D.M. and O'Keefe, S.J., J. Med. Chem., 42 (1999) 2180.
17. Tong, L., Pav, S., White, D.A, Rogers, S., Crane, K.M., Cywin, C.L., Brown, M.L. and Pargellis, C.A., Nat. Struct. Biol., 4 (1997) 311.
18. Wang, Z.L., Canagarajah, B.J., Boehm, J.C., Kassisa, S., Cobb, M.H., Young, P.R., Abdel-Meguid, S., Adams, J.L. and Goldsmith, E.J., Structure, 6 (1998) 1117.
19. Gupta, S.P, Prog. Drug Res., 58 (2002) 223.
20. Akamatsu, M., Curr. Top. Med. Chem., 2 (2002) 1381.
21. Bureau, R., Daveu, C., Lemaitre, S., Dauphin, F., Landelle, H., Lancelot, J.C. and Rault, S., J. Chem. Inf. Comput. Sci., 42 (2002) 962.
22. Liu, H., Ji, M., Luo, X., Shen, J., Huang, X., Hua, W., Jiang, H. and Chen, K., J. Med. Chem., 45 (2002) 2953.
23. Albuquerque, M.G., Hopfinger, A.J., Barreiro, E.J. and de Alencastro, R.B., J. Chem. Inf. Comput. Sci., 38 (1998) 925.
24. Ravi, M., Hopfinger, A.J., Hormann, R.E. and Dinan, L., J. Chem. Inf. Comput. Sci., 41 (2001) 1587.
25. Santos-Filho, O.A. and Hopfinger, A.J., J. Comp. Aided Mol. Des., 15 (2001) 1.
26. Hopfinger, A.J., Wang, S., Tokarski, J.S., Jin, B., Albuquerque, M., Madhav, P.J. and Duraiswami, C., J. Am. Chem. Soc., 119 (1997) 10509.
27. Hong, X. and Hopfinger, A.J., J. Chem. Inf. Comput. Sci., 43 (2003) 324.
28. Iyer, M., Mishru, R., Han, Y. and Hopfinger, A., J. Pharm. Res., 19 (2002) 1611.
29. Krasowski, M.D., Hong, X., Hopfinger, A.J. and Harrison, N.L., J. Med. Chem., 45 (2002) 3210.
30. Berman, H.M., Westbrook, J., Feng, Z., Gilliland, G., Bhat, T.N., Weissig, H., Shindyalov, I.N. and Bourne, P.E., Nucleic Acids Res., 28 (2000) 235 (http://www.rcsb.org/pdb).
31. Insight II User Guide (v.97.0), San Diego, MSI, 1997.
32. Dewar, M.J.S., Zoebisch, E.G., Healy, E.F. and Stewart, J.J.P., J. Am. Chem. Soc., 107 (1985) 3902.
33. 4D-QSAR User's Manual (v.1.00), The Chem21 Group Inc., 1780 Wilson Dr., Lake forest, IL 60045, 1997.
34. MOLSIM User's Guide (v.3.0), Doherty, D. C. and The Chem21 Group Inc., 1780 Wilson Dr., Lake Forest, IL 60045, 1997.
35. Weiner, S.J., Kollman, P.A. and Nguyen, D.T., J. Comput. Chem., 7 (1986) 230.
36. Rogers, D. and Hopfinger, A.J., J. Chem. Inf. Comput. Sci., 34 (1989) 854.
37. Dunn III, W.J. and Rogers D., In Devillers J. (Ed.), Genetic Algorithms in Molecular Modeling. Academic Press, London, 1996.
38. Friedman, J.H., Ann. Stat., 19 (1991) 1.
39. Kubinyi H., In Mannhold R., Krogsgaard-Larsen P. and Timmerman H. (Eds.), Methods and Principles in Medicinal Chemistry, Vol. 1. VHC, Weinheim, 1993.
40. Livingstone, D. Data Analyses for Chemists: Applications to QSAR and Chemical Product Design. Oxford University Press Inc, New York, 1995.